Special Issue Article

Institution of MECHANICAL ENGINEERS
Journal of ENGINEERING TRIBOLOGY

Proc IMechE Part J:
J Engineering Tribology
2014, Vol. 228(9) 916–927

DOI: 10.1177/1350650113517110
pij.sagepub.com
SAGE

Some fundamental aspects of self-levitating sliding contact bearings and their practical implementations

MA Atherton, C Mares and TA Stolarski

Abstract

In this study, fundamental aspects and mechanisms of acoustic levitation together with governing equations are presented first. Then, the acoustic levitation phenomenon is considered as a new way to design air suspension systems capable of self-levitation. A particular emphasis is laid on journal bearings and their specific geometrical configuration. A practical feasibility of using acoustic levitation to separate contacting surfaces is supported and illustrated by results of experimental testing of a number of prototype devices.

Keywords

Self-levitation, squeeze-film action, journal bearing, linear bearing, experimental validation

Date received: 10 July 2013; accepted: 26 November 2013

Introduction

In non-contact bearings, there is no direct physical contact between interacting surfaces. Consequently, these bearings have no wear, almost no friction (except for fluid drag) and they can achieve higher accuracies than conventional rolling-element bearings. Fluid film bearings are the most popular non-contact bearings, whereby a thin film of fluid (liquid or gas) is used to separate the two surfaces. The load-carrying capacity is derived from the pressure within the lubricating film, which can be generated by the motion of the bearing surfaces (self-acting or hydrodynamic/aerodynamic bearings) or by external pressurisation (hydrostatic, or aerostatic) or squeeze motion (squeeze film acoustic bearing, the main focus of this paper), or by a combination of these actions. In addition to fluid film bearings, magnetic bearings are another type of non-contact bearing, which support a load using magnetic levitation force, without the need for a lubricant or separating medium.

Besides existing types of non-contact bearings, acoustic levitation has been used more generally as a means of non-contact suspension of particles. An acoustic wave can exert a force on objects immersed in the wave field and these forces are normally weak but they can become quite large when using high frequency (ultrasonic) and high intensity waves. When these forces are large enough to suspend substances against gravity force then this phenomenon is called acoustic levitation, and since the sound waves used are often in the ultrasonic frequency range (higher than 20 kHz), it is more often called ultrasonic levitation.

Ultrasonic levitation was first used for levitating small particles by creating a standing wave field between a sound radiator and a reflector, namely standing wave ultrasonic levitation. Standing wave type ultrasonic levitators with various features were designed for applications in different scientific disciplines such as container-less material processing and space engineering.[1] Another well-known type of ultrasonic levitation is squeeze film ultrasonic levitation, typically where a flat surface is brought to a conformal radiation surface which vibrates at high frequency. The basic theory underlying the operating principle of ultrasonic levitation together with examples of design embodiments of sliding contacts utilising squeeze-film ultrasonic levitation are presented in this paper.

Department of Mechanical Engineering, School of Engineering and Design, Brunel University, Uxbridge, UK

Corresponding author:
TA Stolarski, Department of Mechanical Engineering, School of Engineering and Design, Brunel University, Kingston Lane, Uxbridge, Middlesex UB8 3PH, UK.
Email: mesttas@brunel.ac.uk

Fundamentals of ultrasonic levitation

Standing wave levitation

The standing wave levitation phenomenon was first observed in Kundt's tube experiment,[2] in which small dust particles moved towards the pressure nodes of the standing wave created in a horizontal (Kundt's) tube. Multiple reflections between an ultrasonic radiator and a solid, flat or concave reflector, generate a standing wave with equally spaced nodes and anti-nodes of the sound pressure and velocity amplitude. Solid or liquid samples with effective diameters less than a wavelength can be levitated below these pressure nodes and so the axial suspension of the sample is an effect of the sound radiation pressure in a standing wave. In addition, when combined with a Bernoulli vacuum component, the sound wave can locate the samples laterally as well.[3]

The first detailed theoretical description of standing wave levitation was given by King,[4] which was extended by Hasegawa and Yosioka[5] to include the effects of compressibility. Embleton[6] adopted King's approach to fit to the case of a rigid sphere in a progressive spherical or cylindrical wave field. Westervelt[7–9] derived a general expression for the force owing to radiation pressure acting on an object of arbitrary shape and normal boundary impedance, and also showed that a boundary layer with a high internal loss can lead to forces that are several orders of magnitude greater than those predicted by the classical radiation pressure theory.

Gorkhov[10] presented a very different approach to King, using a simple method to determine the forces acting on a particle in an arbitrary acoustic field, in which the velocity potential was represented as sum of an incident and a scattered term. Barmatz[11] applied Gorkhov's method to derive the generalised potential and force expressions for arbitrary standing wave modes in rectangular cylindrical and spherical geometries. Lierke[12] gave an overview of standing wave acoustic levitation based on long-term research and development activities of the European and the US space agencies. Xie and Wei[13] studied the acoustic levitation force on disk samples and the dynamics of large water drops in a planar standing wave, by solving the acoustic scattering problem through incorporating the boundary element method.

The theoretical approach of King[4] is presented below for understanding the basic working principles of standing wave levitation. Assuming that the working fluid is adiabatic and barotropic, the equations of motion can be written as

$$\rho\frac{Du}{Dt}=-\frac{\partial p}{\partial x},\ \rho\frac{Dv}{Dt}=-\frac{\partial p}{\partial y},\ \rho\frac{Dw}{Dt}=-\frac{\partial p}{\partial z} \tag{1}$$

where $\frac{D}{Dt}=\frac{\partial}{\partial t}+u\frac{\partial}{\partial x}+v\frac{\partial}{\partial y}+w\frac{\partial}{\partial z}$ is the absolute derivative, ρ the density of the medium, p the pressure and (u, v, w) the Cartesian velocity components.

By defining $\varpi = {}^{dp}/_{\rho}$ the equation of motion can be rewritten as

$$\frac{Du}{Dt}=-\frac{\partial\varpi}{\partial x},\ \frac{Dv}{Dt}=-\frac{\partial\varpi}{\partial y},\ \frac{Dw}{Dt}=-\frac{\partial\varpi}{\partial z} \tag{2}$$

When the motion is non-rotational, the velocity components can be expressed in terms of the velocity potential ϕ

$$(u, v, w)=-\nabla\phi \tag{3}$$

In the case where air is the medium, the velocity potential can be obtained from the approximate linear wave equation

$$\nabla^2\phi=\frac{1}{c^2}\frac{\partial^2\phi}{\partial t^2} \tag{4}$$

which is simplified from the exact differential equation for ϕ using a second-order approximation. The equation of continuity is

$$\frac{\partial\rho}{\partial t}+\frac{\partial}{\partial x}(\rho u)+\frac{\partial}{\partial y}(\rho v)+\frac{\partial}{\partial z}(\rho w)=0 \tag{5}$$

and the pressure variation can then be derived from equation (5) as

$$\Delta p=p-p_0=p_0\frac{\partial\phi}{\partial t}+\frac{1}{2}\frac{\rho_0}{c^2}\left(\frac{\partial\phi}{\partial t}\right)^2-\frac{1}{2}\rho_0 q^2 \tag{6}$$

where ρ_0 is the density of the surrounding medium, ϕ is the velocity potential, c is the sound speed in air and q is the velocity amplitude equal to $\sqrt{u^2+v^2+w^2}$. Detailed derivation of equation (6) can be found in King.[4] The time-averaged acoustic pressure on a rigid body can be calculated by integrating the acoustic pressures acting on each surface element of the body. In the case of a plane standing wave, the velocity potential ϕ_s can be expressed as[4]

$$\phi_s=|A|\cos kh\cos\omega t \tag{7}$$

where $|A|$ is the amplitude of the velocity potential, $k=2\pi/\lambda$ is the wave number and h is the position where the sphere, which is assumed to be small, is located. The acoustic radiation force on a rigid sphere can be calculated as

$$F=-\frac{5}{6}\pi\rho_0|A|^2(kR_s)^3\sin(2kh) \tag{8}$$

with R_s being the radius of the sphere.

Bucks and Muller[14] presented the first experimental setup for positioning of small samples in acoustic standing waves, in which a small particle was trapped

at a position slightly below the pressure nodes of the standing wave between a radiator and a reflector. Wang et al.[15] presented an acoustic chamber for positioning of molten materials in an extreme temperature gradient. Whymark[16] proposed an acoustic levitator for positioning of materials in space using a single source of sound that achieved fine position control by adjusting the reflector. Lierke[17] presented an acoustic levitator for positioning materials samples in mirror furnaces when processing in space. Trinh[18] presented a compact acoustic levitation device for microgravity studies of fluid dynamics and materials science. This classic structure was later modified to achieve better performance. Otsuka et al.[19] used a stepped circular vibrating plate as a radiator for producing high-intensity ultrasound fields which was different from conventional piston-like vibration sources in using the flexural vibration mode of the plate with two nodal rings to achieve higher vibration amplitude. The stepped plate has a concave channel with fixed depth equal to the half sound wavelength in air. This special design makes the concave and convex blocks vibrate in the counter phase so that the ultrasound propagating in the air is modulated in the same phase. As a result, a narrow, intensive, high directional ultrasound beam is obtained. Xie and Wei[20] enhanced the standing wave acoustic levitation force by properly curving the surface and enlarging the reflector and thus high density material, e.g. tungsten, was successfully levitated for the first time using standing wave ultrasonic levitation. Recently Xie and Wei[21] reported the successful levitation of small living animals such as an ant, ladybird and small fish with a standing wave acoustic levitator and their experiments showed that the vitality of the small animals was not impaired during levitation.

All the standing wave levitation systems presented above possessed the classic radiator-reflector configuration and so applications of such configuration were limited to the levitation of small particles whose dimension does not exceed the wavelength of the imposed sound wave. Moreover, the levitation force obtainable from this configuration is very limited and therefore modifications and improvements are needed before standing wave ultrasonic levitation can be applied in non-contact suspension systems such as linear and rotational bearings.

Squeeze-film ultrasonic levitation

Salbu[22] reported a levitation system for objects with flat surfaces that used magnetic actuators to excite two conforming surfaces oscillating next to each other to generate a positive load-supporting force. In 1975, Whymark[16] reported that a brass planar disk of 50 mm in diameter and 0.5 mm in thickness was levitated extremely close to a piston vibration source driven harmonically at a frequency of 20 kHz. These levitation effects reported by Salbu and Whymark were named as squeeze-film levitation and also called near-field acoustic levitation.

A schematic diagram of squeeze-film levitation system usually consists of two parallel plates separated by an air film of thickness h_0. The time-averaged mean pressure in the gap has a value which is higher than the surroundings, which is caused by the second-order effects possessed by the rapidly squeezed and released gas film between two plane surfaces. Two distinct properties distinguish this type of levitation from standing-wave levitation. First, the reflector is no longer needed; instead, the levitated object itself acts as an obstacle for the free propagation of the ultrasonic wave-front. Second, the gap between radiation source and the levitated object must be much smaller than the sound wavelength in air. Thus, instead of a standing wave, a thin gas film is formed between the radiator and the levitated object, which is rapidly squeezed and released. A simple model introduced by Wiesendanger[23] is presented here to demonstrate the basic idea of how squeeze-film levitation works. The leaking and pumping at the boundary is neglected in this model, thus only the trapped gas that is rapidly squeezed and released is considered. The total mass of air in a fixed volume remains constant, resulting in

$$pV^n \approx ph^n = \text{const} \tag{9}$$

where p represents the pressure, V the volume of the trapped gas, h the gap distance for a one-dimensional contact and n the polytropic constant ($n=1$ for isothermal condition, $n=k\approx 1.4$ for an adiabatic condition of air). The relation between pressure and levitation distance is nonlinear, which leads to a distorted pressure $p(t)$ resulting from the imposed periodic gap distance $h(t)$. The gap distance (air film thickness) oscillates harmonically around a equilibrium position, h_0, i.e.

$$h(t) = h_0(1 + \varepsilon \sin \omega t) \tag{10}$$

in which ω is the angular frequency of the oscillation, ε the excursion ratio ($\varepsilon = a_0/h_0$). The excursion ratio denotes the ratio of the vibration amplitude over the mean gap distance, where a_0 is the vibration displacement amplitude. The mean pressure under isothermal conditions ($n=1$) can be expressed as in[23]

$$\bar{p} = \frac{p_0 h_0}{2\pi} \int_0^{2\pi} \frac{1}{h(t)} \mathrm{d}(\omega t) = \frac{p_0}{\sqrt{1-\varepsilon^2}} \tag{11}$$

It can be easily seen that mean pressure $\bar{p}$ exceeds the ambient pressure, p_0. The harmonic motion of the radiating surface produces a non-harmonic pressure

oscillation whose mean value is not equal to the quasi-static value, p_0. The positive mean pressure $\bar{p}$ is larger than the ambient pressure, p_0, which is a qualitative confirmation of the existence of a levitation pressure. However, to obtain a quantitative value of the levitation pressure, more sophisticated models are needed which take into account the boundary conditions such as the pressure release at the edge of the gap. Such a model of squeeze-film levitation can be established by following two different routes: acoustic radiation pressure theory and gas film lubrication theory. The first one modifies the acoustic radiation pressure theory according to the different physical conditions in squeeze-film levitation. The second one starts from the theory of gas film lubrication since the working principle is actually similar.[24,25] Gas film lubrication has been investigated for many years in micro-mechanical systems commonly by solving Reynolds equation.

A simplified equation for the radiation pressure in squeeze-film acoustic levitation was derived from the acoustic radiation pressure theory presented by Chu and Apfel[26] by Hashimoto et al.[27] They calculated the Rayleigh radiation pressure in an ideal gas on a perfectly reflecting target as

$$p = \langle P - P_0 \rangle = \frac{1+\gamma}{2}\left(1 + \frac{\sin(2kh)}{2kh}\right)\langle E \rangle \tag{12}$$

Here, E is the energy density which can be expressed as

$$E = \left(\frac{a_0^2}{4}\right)\left(\frac{\rho_0 \omega^2}{\sin^2(kh)}\right) \tag{13}$$

in which k represents the wave number, γ a specific heat ratio, ω the angular velocity of the wave, a_0 the vibration amplitude and h the distance between vibration source and target. In squeeze film levitation, the levitation distance is very small compared to the wavelength of sound in the free field. It ranges from several to several tens micrometers, therefore in equation (12) $\sin kh \approx kh$ was simplified to a linear equation for the radiation pressure in squeeze film levitation

$$\Psi = \frac{1+\gamma}{4}\rho_0 c^2 \frac{a_0^2}{h^2} \tag{14}$$

The radiation pressure, Ψ, in squeeze film levitation is inversely proportional to the square of the levitation distance and proportional to the square of the vibration amplitude a_0. Hashimoto et al. did experiments to verify equation (14) and the results for maximum levitation force were 25% lower than those calculated from equation (14). The authors put this discrepancy down to the finite dimensions of the surfaces and the non-uniformity of the amplitude of the radiation surface.

Wiesendanger[23] also used gas film lubrication theory[24,25] and solved the general Reynolds equation both analytically and numerically to achieve quantitative results for the levitation forces. Nomura and Kamakura[28] theoretically and experimentally examined squeeze-film acoustic levitation by numerically solving the basic equations of a viscous fluid using MacCormack's finite-difference scheme and including viscosity and acoustic energy leakage in the model. Minikes[29] studied the levitation force induced by pressure radiation in gas squeeze films, investigating the flow induced both by vibrations perpendicular to a flat surface and by a flexural wave propagating parallel to the surface. For the first case, numerical and second-order analytical perturbation solutions were compared and proved to be in good agreement to each other. For the second case, a modified Reynolds equation was derived to obtain the pressure distribution and the velocity profile in the film in order to determine the reaction forces. Later, Minikes[30] examined the validity of the pressure release boundary condition and the isothermal assumptions through a CFD scheme. By comparing his results to a one-dimensional analytical solution, Minikes found that the levitation force reduced to a half when the energy leakage near the edges of the levitated object were taken in to account. This indicates that the assumption of pressure release at the boundaries, implied in the Reynolds equation, is inadequate in cases where the driving surface is significantly larger than the levitated surface.

Squeeze-film ultrasonic levitation with inertia effect

In depth analysis of the significance of inertia effect in squeeze-film pressure generation was carried out by Stolarski and Chai,[31] based on the Reynolds equation modified to include an inertia effect. Therefore, in order to avoid unnecessary repetition, only selected equations are presented here as a comprehensive treatment of the problem is given elsewhere.[31] In the case of a linear bearing configuration (discussed in more details later), air film geometry can be represented as in Figure 1. Cyclic movement $e\sin(\omega t)$ in the vertical direction (z-axis) generates a characteristic air velocity given by $w \approx e\omega$, where w is flow velocity of air in z direction, e is the amplitude of vibration of a squeeze surface produced by a piezoelectric actuator, and ω denotes angular velocity of the squeeze surface rotation. The order of magnitude of the average flow rate Q due to squeeze action over all the boundaries can be determined, approximately, from the expression below (for derivation details see Stolarski and Chai[31])

$$u \approx \frac{3Q}{14 l_o h_o} = \frac{3 w l_o b}{14 l_o h_o} = \frac{3wb}{14 h_o} = \frac{3e\omega b}{14 h_o} \tag{15}$$

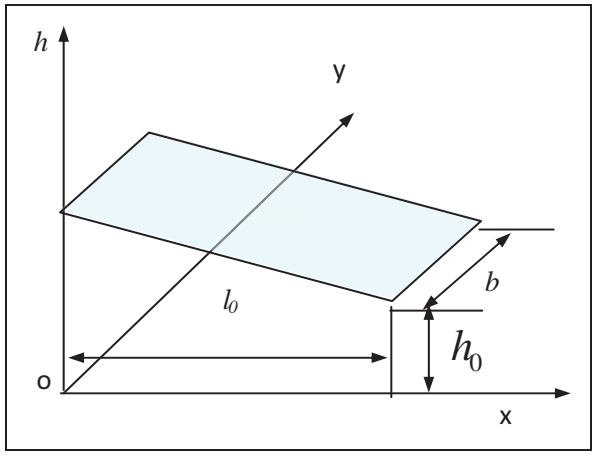

Figure 1. Diagram showing air film dimensions.

Therefore,

$$\frac{w}{u} \approx \frac{14e\omega h_o}{3e\omega b} \approx \frac{h_o}{b} \approx \psi < 0.001 \tag{16}$$

This value implies that the velocity in the vertical direction (see Figure 1) is a small quantity of a higher order. This inference is applied to the Navier–Stokes equation, given below in a simplified form by one order of magnitude

$$\frac{\partial p}{\partial x} = \frac{\partial}{\partial z}\left(\mu \frac{\partial u}{\partial z}\right);\ \frac{\partial p}{\partial y} = \frac{\partial}{\partial z}\left(\mu \frac{\partial v}{\partial z}\right);\ \frac{\partial p}{\partial z} = 0 \tag{17}$$

In order to find out that the inertia effect in the vertical direction (air film thickness direction) is negligible compared to that in x- and y-axes direction, modified Navier–Stokes equations with inertia terms given below are used

$$\rho \frac{Du}{Dt} = \rho\left(u\frac{\partial u}{\partial x} + v\frac{\partial u}{\partial y} + w\frac{\partial u}{\partial z} + \frac{\partial u}{\partial t}\right) \tag{18}$$

$$\rho \frac{Dv}{Dt} = \rho\left(u\frac{\partial v}{\partial x} + v\frac{\partial v}{\partial y} + w\frac{\partial v}{\partial z} + \frac{\partial v}{\partial t}\right) \tag{19}$$

$$\rho \frac{Dw}{Dt} = 0 \tag{20}$$

Therefore, equations given by (17) can be replaced by

$$\rho \frac{Du}{Dt} + \frac{\partial p}{\partial x} = \frac{\partial}{\partial z}\left(\mu \frac{\partial u}{\partial z}\right) \tag{21}$$

$$\rho \frac{Dv}{Dt} + \frac{\partial p}{\partial y} = \frac{\partial}{\partial z}\left(\mu \frac{\partial v}{\partial z}\right) \tag{22}$$

$$\frac{\partial p}{\partial z} = 0 \tag{23}$$

Terms $\rho\frac{Du}{Dt}$ and $\rho\frac{\mathrm{Dv}}{\mathrm{Dt}}$ relate to non-linear flow velocity in equations (21) and (22) and cannot be integrated to determine velocities u and v. The thickness of an air film developed within the squeeze contact is small, so averaging the inertia effect across the film thickness is permissible. Thus

$$\rho \frac{Du}{Dt} \approx \rho\left(\frac{1}{h}\int_0^h \frac{Du}{Dt}\mathrm{d}z\right) \tag{24}$$

$$\rho \frac{Dv}{Dt} \approx \rho\left(\frac{1}{h}\int_0^h \frac{Dv}{Dt}\mathrm{d}z\right) \tag{25}$$

Combining equations (24) and (25) with equations (21) and (22) results in

$$\mu \frac{\partial^2 u}{\partial z^2} = \rho\left(\frac{1}{h}\int_0^h \frac{Du}{Dt}\mathrm{d}z\right) + \frac{\partial p}{\partial x} \tag{26}$$

$$\mu \frac{\partial^2 v}{\partial z^2} = \rho\left(\frac{1}{h}\int_0^h \frac{Dv}{Dt}\mathrm{d}z\right) + \frac{\partial p}{\partial y} \tag{27}$$

$$\frac{\partial p}{\partial z} = 0 \tag{28}$$

The use of the idea of 'averaged inertia' results in a number of equations in which the inertia emerges as a modification term. Mass flow rate per unit length of the contact can be estimated from

$$q_n = \left(\frac{-h^3\rho}{12\mu}\frac{\partial p}{\partial n}\right) + \left(\frac{-h^2\rho^2}{12\mu}\int_0^h \frac{Du_n}{Dt}\mathrm{d}z\right) = q_n^0 + q_n^1 \tag{29}$$

The first term, q_n^0, denotes contents of the first bracket and the second, q_n^1, symbolises the expression in the second bracket. According to equation (29) the flow rate consists of the flow caused by the pressure gradient, q_n^0, and the flow due to inertia, q_n^1. The Reynolds equation can be arrived at by integration of the continuity equation across the film thickness

$$\frac{\partial q_x}{\partial x} + \frac{\partial q_y}{\partial y} + \frac{\partial(\rho h)}{\partial t} = 0 \tag{30}$$

where q_x and q_y are mass flow rates per unit length in Cartesian co-ordinate system.

Selecting an infinitesimal area Ω in the xy plane enclosed by the boundary Γ, one can further integrate equation (30) to obtain

$$\int_\Gamma q_n \mathrm{d}\Gamma + \int\int_\Omega \frac{\partial(\rho h)}{\partial t}\mathrm{d}\Omega = 0 \tag{31}$$

In the above equation, q_n symbolises mass flow rate normal to boundary Γ. According to equation (31)

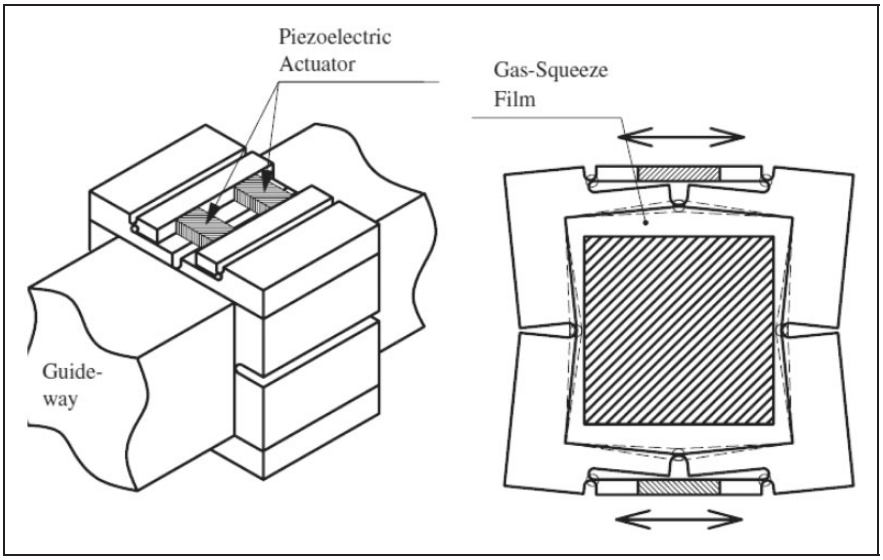

Figure 2. Schematic of the linear bearing configuration.

the mass flow rate through the boundary Γ is equal to the mass reduction rate in the domain Ω. Involving the inertia effect contained in equation (29) with equation (31) leads to a boundary integral equation of the form

$$\int_{\Gamma} (q_n^0 + q_n^1) \mathrm{d}\Gamma + \int \int_{\Omega} \frac{\partial (\rho h)}{\partial t} \mathrm{d}\Omega = 0 \qquad (32)$$

Examples of design embodiments of self-levitating sliding contacts

This paper is concerned with the important application of squeeze-film levitation to developing non-contact linear and rotational bearings. A number of examples of possible practical implementation of the fundamental principles of squeeze-film ultrasonic levitation are presented and briefly discussed in this section.

Linear motion bearing

Precision linear motion is required in a number of practical applications. One example is lithography where silicon chip to be engraved with a circuit has to be repositioned with nano-metre accuracy. Figure 2 depicts a linear bearing concept consisting of a specially shaped frame and a guiding beam of square cross-section. The geometry of the frame has been selected to have the maximum levitating effect by producing deformation of its three sides by means of 'elastic hinges'.

Figure 3, being a model for finite element (FE) analysis, shows the geometry of the frame in more detail. When in a deformed state within its elastic limits, the frame creates converging gaps with a flat and un-deformable guide, hence facilitating formation of an air film/pocket. When constant and

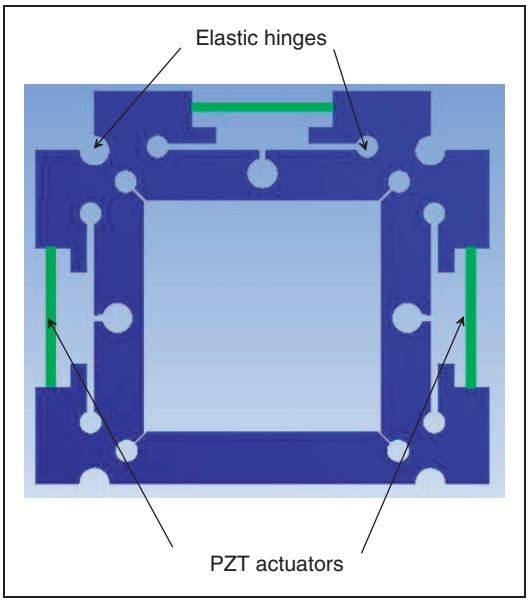

Figure 3. Geometry details of the frame.

periodically changeable deformations of the frame are generated at a suitable frequency (around 5 kHz) a squeeze-film mechanism comes into operation and a pressure is created that is able to separate the frame from the guide. The load capacity of such a bearing is not very impressive (a few Newtons), nevertheless for special applications such as contactless paper transportation and lithography, the force is sufficient.

Modelling of the linear motion bearing (floating frame) is based on the Reynolds equation appropriately modified to account for the specific geometry (see Figure 4).

$$\frac{\partial}{\partial X}\left[H^3 P \frac{\partial P}{\partial X}\right] + \frac{\partial}{\partial Z}\left[H^3 P \frac{\partial P}{\partial Z}\right] = \sigma \frac{\partial (PH)}{\partial T} \qquad (33)$$

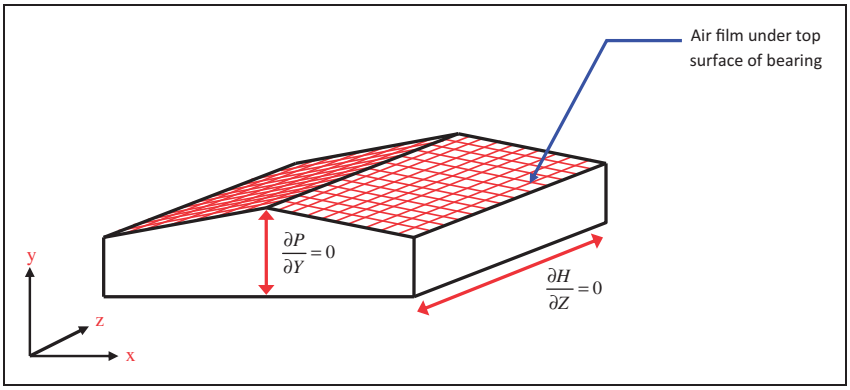

Figure 4. Discretisation of the problem.

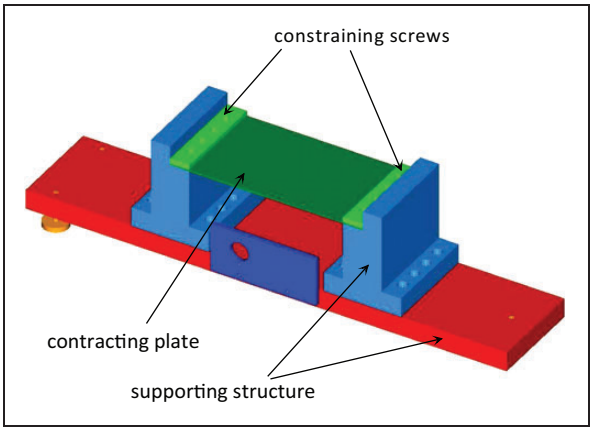

Figure 5. Computer-created image of the floating pad testing set-up.

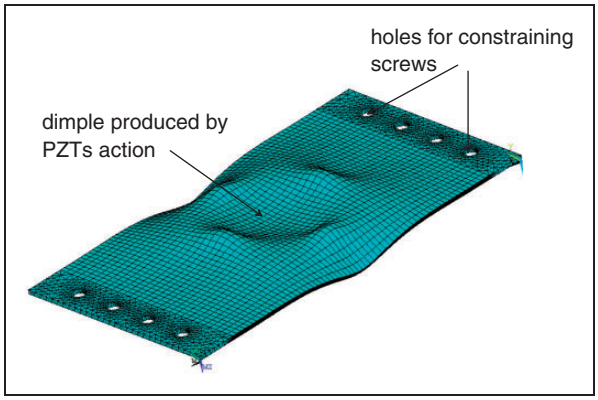

Figure 6. FE image of the plate in deformed state.

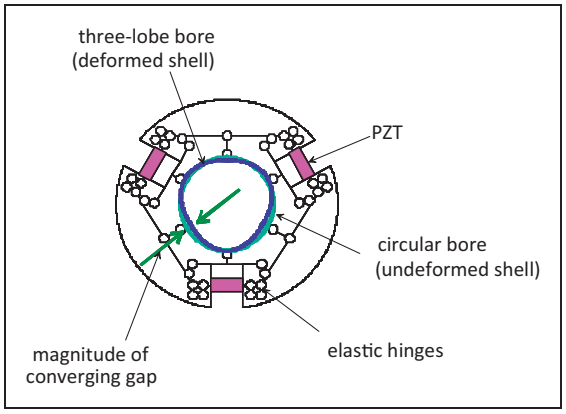

Figure 7. Diagram showing geometry, 'elastic hinges' and arrangement for PZTs.

where σ is the squeeze number. Equation (33) can be expanded to give

$$PH^3\frac{\partial^2 P}{\partial X^2}+H^3\left[\frac{\partial P}{\partial X}\right]^2+3PH^2\frac{\partial P}{\partial X}\frac{\partial H}{\partial X}+PH^3\frac{\partial^2 P}{\partial Z^2}+H^3\left[\frac{\partial P}{\partial Z}\right]^2+3PH^2\frac{\partial P}{\partial Z}\frac{\partial H}{\partial Z}=\sigma P\frac{\partial H}{\partial T}+\sigma H\frac{\partial P}{\partial T} \quad (34)$$

Assuming constant film thickness along the z-axis, $\frac{\partial H}{\partial Z}=0$ (see Figure 4), part of the equation (34) can be omitted and solved using known numerical algorithms.

Floating pad

Converging gap geometry necessary for the squeeze-film mechanism can also be achieved by the use of a contraction effect usually represented by Poisson's ratio characteristic for a given material. The arrangement for practical implementation of the contraction effect combined with the squeeze-film mechanism is shown in Figure 5.

An array of PZTs is fixed to the back side of the contracting plate and under the action of PZTs the plate deforms as shown in Figure 6.

The dimple is a result of the plate's contraction in the vertical direction due to its elongation in the horizontal direction (Poisson's effect). Cyclic fluctuation of the dimple with appropriate frequency creates

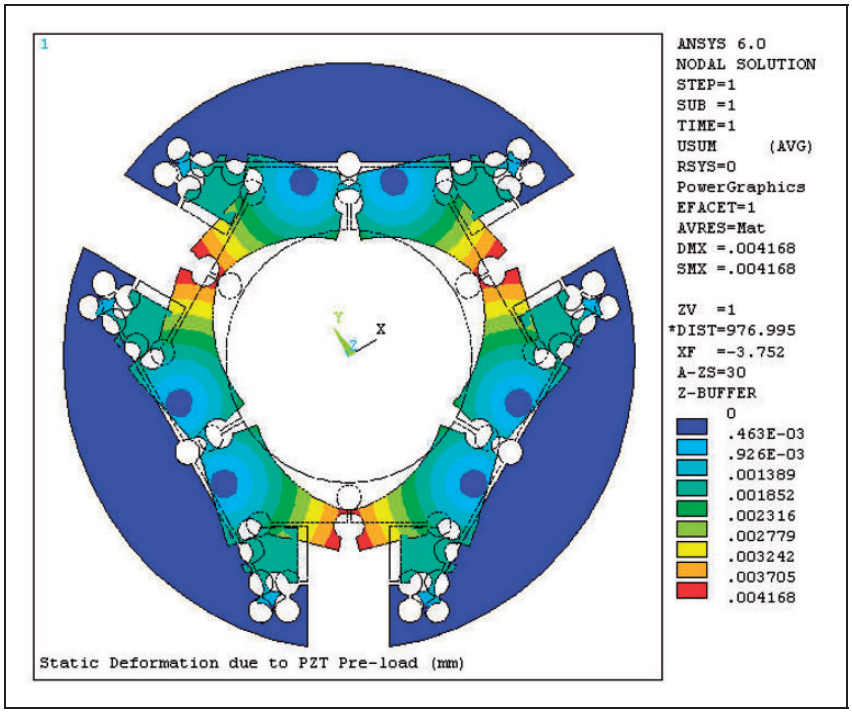

Figure 8. FE model showing stress map of the bearing shell in deformed state. Three-lobe geometry can be clearly seen.

conditions necessary for the squeeze-film operation and generation of pressure at the interface between the plate and an object to be levitated.

Modelling of the floating pad for analysis purpose starts with determining the modes of the plate's deformation. Only those modes of deformation producing geometry favourable for the squeeze-film mechanism should be selected. An easy way to carry out structural deformation analyses is to use finite element analysis.

Once the required geometry of deforming plate is secured, the squeeze-film effect equations can be employed to determine pressure in the air film and hence load capacity of the floating pad. The effectiveness of squeeze-film ultrasonic levitation can be assessed from

$$\nabla[H^3 P \bullet \nabla P] = \sigma \frac{\partial (PH)}{\partial T} \tag{35}$$

In fact equation (35) is the Reynolds equation in non-dimensional variables, which are defined as follows

$$X = \frac{x}{l_0},\ Y = \frac{y}{l_0},\ H = \frac{h}{h_0},\ P = \frac{p}{p_a},\ T = \omega_0 t,$$

$$\sigma = \frac{12\eta\omega_0 l_0^2}{p_a h_0^2}$$

Here H is the separation distance, P is the pressure, T is the time, l_0 is the lateral dimension of the pad, h_0 is the mean air film thickness, p_a is the ambient air pressure, η is the viscosity of air and σ is the squeeze number. The squeeze number is an important factor

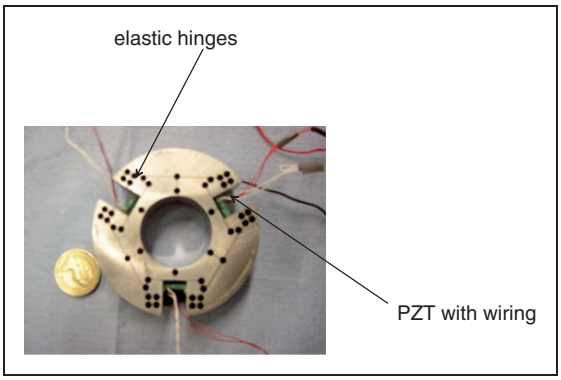

Figure 9. Photograph of the bearing shell with 'elastic hinges'. One pound coin shown illustrates the physical size of the shell.

in finding the load capacity of a bearing operating with squeeze-film ultrasonic levitation. Low σ means that the air is simply flowing through the contact without undergoing compression and decompression. High σ signifies a relatively stationary air film undergoing cyclic compression and decompression and hence contributing to the load capacity of the contact.

Rotating motion bearing

Early attempts to design rotating motion bearing operating on squeeze-film ultrasonic levitation principle utilised elaborate geometry for the bearing shell. An example is shown in Figure 7 and an FE model of the bearing shell with stress map for its deformed state is depicted in Figure 8.

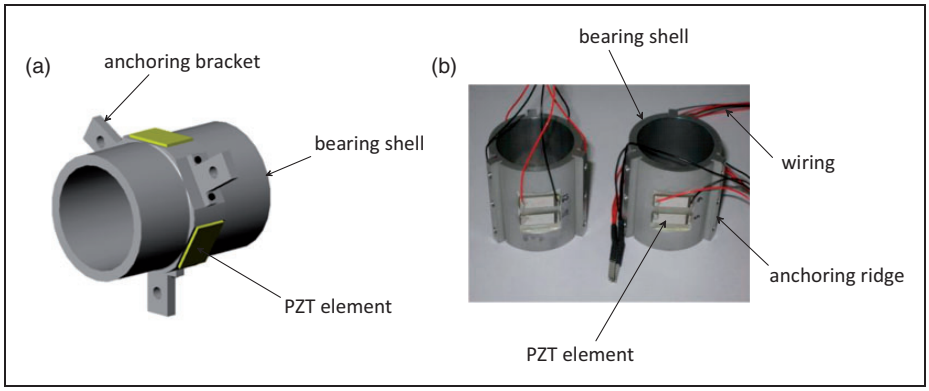

Figure 10. Two examples of possible geometrical configurations of bearings operating on squeeze-film ultrasonic levitation principle: (a) design One; (b) design Two.

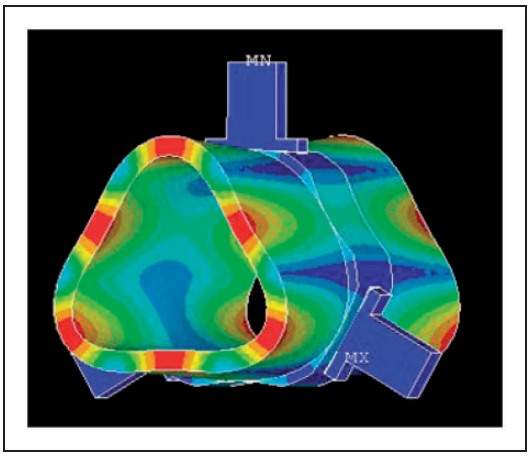

Figure 11. Finite element model of the shell in deformed state.

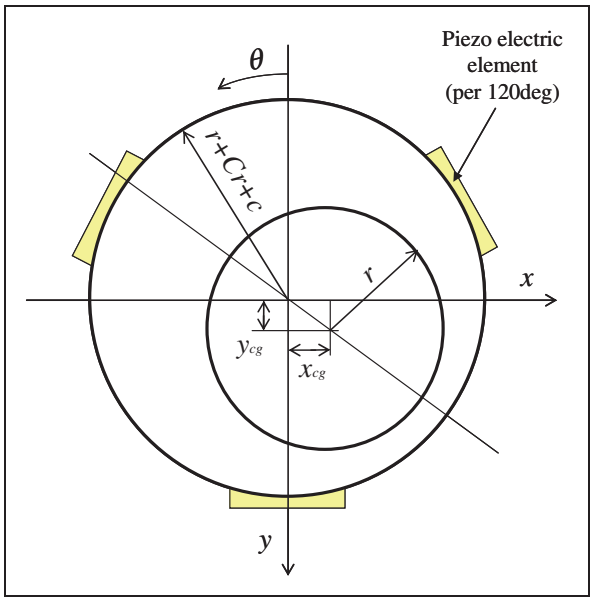

Figure 12. Geometry of the bearing used to express air film thickness analytically.

The photograph in Figure 9 shows an actual bearing made of bronze. It can be seen that there are a number of small holes and cuts which, together, constitute 'elastic hinges' whose main function is to make the bearing shell more elastic and deformable under the action of the PZTs. It should also be noted that this bearing is an early design having quite thick walls and operating at subsonic frequencies.

The latest design of bearing is simpler to make as it does not have such an elaborate array of holes and cuts. Figure 10 shows two possible configurations.

An FE model of the bearing of Design One (see Figure 11) depicts the bearing's shell in a deformed state. Again, one can clearly see that the circular bore of the shell is transformed into a three-lobe shape under the action of the PZTs. In the case shown by Figure 11 the frequency of cyclic deformation was 21.6 kHz.

Computer modelling of a rotating bearing operating on the squeeze-film ultrasonic levitation principle is based on an appropriately modified Reynolds' equation given by equation (30). However, the very small thickness of the air film developed within the bearing, warrants neglecting the inertia effect of the film across its thickness.[31]

Using geometry depicted in Figure 12, the air film thickness can be represented by the following expression

$$h = C_r + x_{cg}\sin\theta + y_{cg}\cos\theta + c(\theta, z, t) \tag{36}$$

The term, c(θ, z, t) on the right-hand side of equation (36) represents the contribution of cyclic deformation of the bearing's shell to the formation of the air film. Equations (30) and (36) constitute fundamentals of a rotating motion bearing operating on squeeze-film ultrasonic levitation. They can be solved numerically with the help of experimentally measured elastic deformations of the bearing's shell induced by the PZTs.

Experimental confirmation of the concepts

In order to demonstrate the feasibility of squeeze-film ultrasonic levitation preliminary experimental testing of design embodiments presented earlier was undertaken. Undoubtedly the most useful information, in view of potential practical applications, is the load-carrying capacity. Some selected results obtained from preliminary experimental testing are presented in this section.

Floating pad

Figure 13 shows pressure, synonymous with the load-carrying capacity, developed within the context of the configuration shown in Figure 5. The plate made of aluminium was 200 mm long, 100 mm wide and had a thickness of 1.9 mm. The frequency used to excite the plate was 25.6 kHz. In this figure the separation distance (amount of levitation of the object above the fixed and vibrating aluminium plate) is plotted versus the inverse of the root of the total mass of the levitating object. A clear linear relationship is present between the levitation distance and the inverse root of the applied mass. This relationship appears very strong as the straight line fits rather well with all the data points, even with the points where the separation distances are less than 5 μm. Additionally, experiments showed that the change of plate material, plate vibration frequency, amplitude and offset voltage results in different applied load versus separation distance characteristic. Details concerning experimental techniques used to generate results plotted in Figure 13 are given elsewhere. Details concerning experimental techniques used to plot results shown in Figure 13 are given in Woolliscroft.[32]

Linear motion bearing

Figure 14 illustrates the experimentally measured load capacity of the linear motion bearing (expressed as air film thickness) with configuration and geometry as shown in Figure 3.[34] A clear trend of film thickness reduction with applied load is demonstrated. The expected input amplitude trend occurred with larger input amplitudes sustaining a thicker air film under the same load. As with the floating pad contact, performance of the linear motion bearing depends on the frequency of cyclic deformation, offset voltage and amplitude. Moreover, it was found during experimental testing that the bearing is quite sensitive to the surface finish of its squeeze-film generating areas. Details concerning experimental techniques used to generate results plotted in Figure 14 can be gleaned from Woolliscroft[33] and Taghipourfard.[34]

Rotating motion bearing

As an illustration of the performance of a rotating motion bearing utilising squeeze-film ultrasonic levitation the load-bearing capacity, experimentally

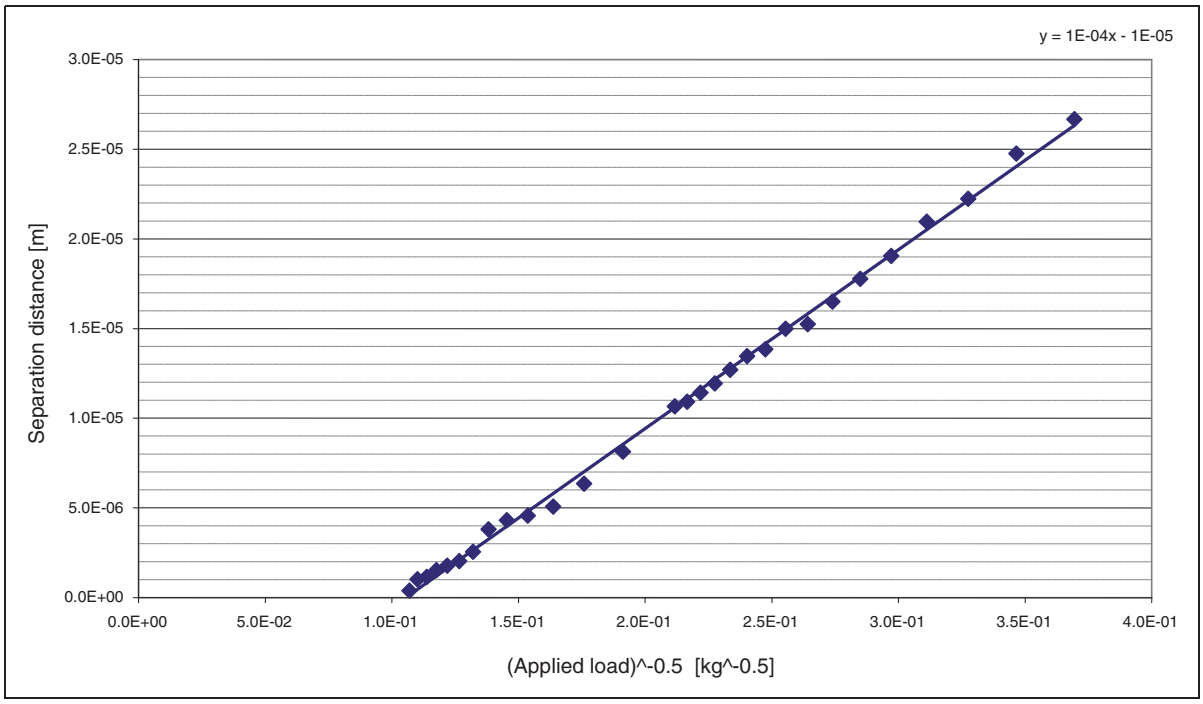

Figure 13. Separation distance vs inverse root of the total mass of the levitation object. A linear relationship is found.

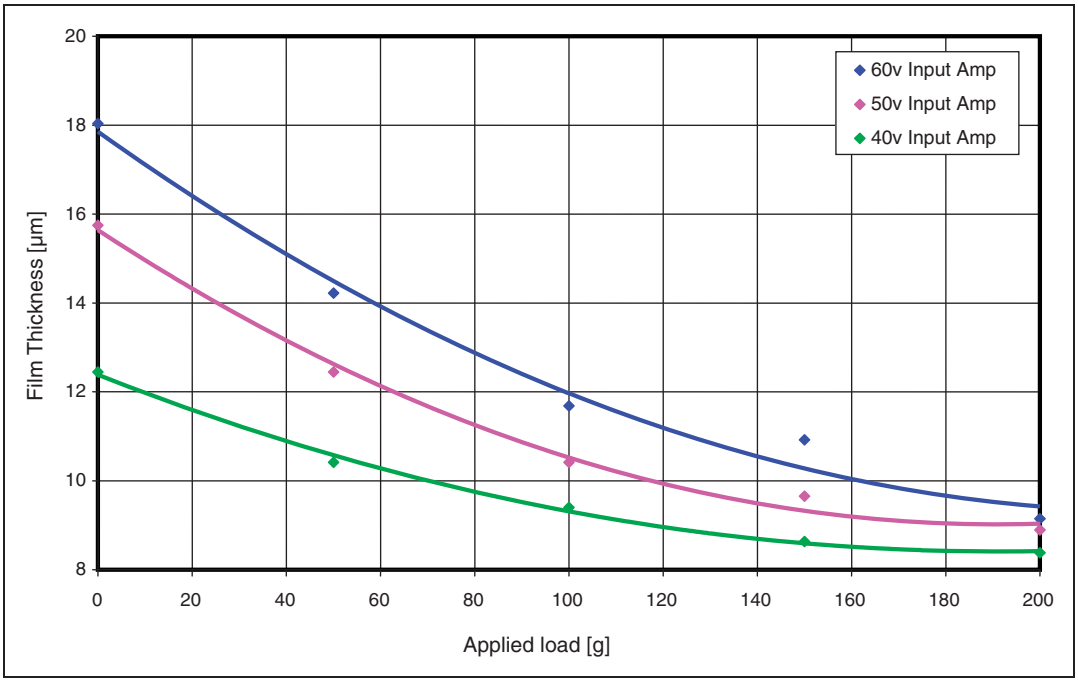

Figure 14. Bearing load capacity results at 2600 Hz and 70 V off-set.

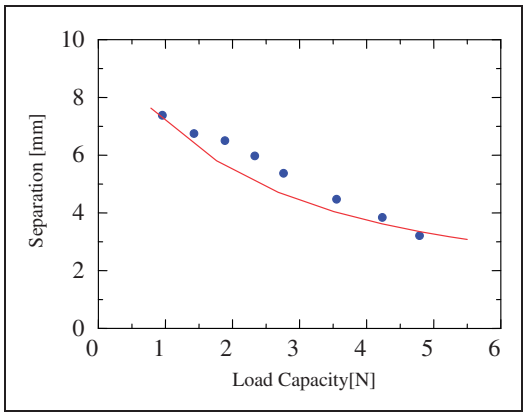

Figure 15. Comparison of computer predicted load capacity (continuous line) with experimentally determined load capacity (filled circles).

determined, is shown. Figure 15 depicts the relationship between applied load on the bearing and the separation of the shaft from the bearing shell (air film thickness). The continuous line represents load capacity predicted by a computer model and the filled circles represent experimentally determined load capacity. The tested bearing of geometry shown in Figure 10(a) was made of aluminium 50 mm in length and 30 mm nominal bore diameter. The diametral clearance was 20 µm. A typical resonant frequency at which the bearing achieved the highest load capacity was in the order of 30–35 kHz. Computer prediction was obtained by solving numerically (Newton–Raphson iteration) a suitably modified Reynolds equation. Although the load capacity is not huge, nevertheless it is real and measurable and might be of sufficient magnitude for certain specialist applications. Details concerning experimental techniques used to generate results plotted in Figure 13 can be obtained from Stolarski et al.[35]

Concluding summary

Self-levitating non-contact bearings (with rotational or linear motion) offer significant advantages in many applications. Due to its non-contact principle, the system can run at much higher speeds than conventional sliding contact bearings. Also, problems such as excessive temperature or wear of the bearing components would be avoided. Squeeze-film ultrasonic levitation can be accomplished in a number of ways through different geometries of bearing configuration dependent on the type of motion desired. Load-carrying capacities of this new class of bearings are, at the moment, rather low although there is scope to increase this by means of careful selection of geometry, materials, frequency and amplitude of vibration, and the power of PZT actuators. Likewise, computer modelling of this type of bearings is a dynamically evolving area of research. More accurate performance prediction, important at the bearing design stage for a particular application, is achievable as more factors governing the acoustic pressure generation are incorporated into theoretical analyses. This paper has demonstrated the feasibility of squeeze-film ultrasonic levitation to be used in a number of bearing embodiments depending on the requirements of the practical application.

Funding

This work was partially supported by the Engineering and Physical Sciences Research Council, UK (grant number EP/F04979X/1).

Conflict of interest

None declared.

References

1. Vandaele V, Lambert P and Delchambre A. Non-contact handling in micro assembly: Acoustical levitation. *Precis Eng* 2005; 29: 491–505.
2. Poynting JH and Thomson JJ. *A textbook of physics*. London: Charles Griffin & Co., 1904.
3. Daidzic N. *Nonlinear droplet oscillations and evaporation in an ultrasonic levitator*. PhD Thesis, Friedrich-Alexander University, Erlangen, 1995.
4. King LV. On the acoustic radiation pressure on spheres. *Proc R Soc Ser A Lond* 1934; 147: 212–240.
5. Hasegawa T. Acoustic-radiation force on a solid elastic sphere. *Acoust Soc Am* 1969; 46: 1139.
6. Embleton TFW. Mean force on a sphere in a spherical sound field. *Acoust Soc Am* 1954; 26: 40–48.
7. Westervelt PJ. The mean pressure and velocity in a plane acoustic wave in a gas. *Acoust Soc Am* 1950; 22: 319–327.
8. Westervelt PJ. The theory of steady forces caused by sound waves. *Acoust Soc Am* 1951; 23: 312–315.
9. Westervelt PJ. Acoustic radiation pressure. *Acoust Soc Am* 1957; 29: 26–29.
10. Gorkhov LP. On the forces acting on a small particle in an acoustical field in an ideal fluid. *Sov Phys Dokl* 1962; 6: 773–781.
11. Barmatz M and Collas P. Acoustic radiation potential on a sphere in plane, cylindrical, and spherical standing wave fields. *Acoust Soc Am* 1985; 77: 928–945.
12. Lierke EG. Acoustic levitation a comprehensive survey of principles and applications. *Acta Acustica* 1996; 82: 12–19.
13. Xie WJ and Wei B. Dynamics of acoustically levitated disk samples. *Phys Rev* 2004; 70: 4–13.
14. Bucks K and Muller H. Uber einige Beobachtungen an schwingenden Piezoquarzen und ihrem Schallfeld. *Z Phys* 1933; 84: 75–86.
15. Wang TG and Saffren MM. Acoustic chamber for weightless positioning. *AIAA J* 1974; 155: 213–221.
16. Whymark RR. Acoustic field positioning for containerless processing. *Ultrasonics* 1975; 13: 251–261.
17. Lierke LG, Grossbach R and Clancy P. Acoustic positioning for space processing of materials science samples in mirror furnaces. In: *IEEE ultrasonic symposium proceedings*, Atlanta, GA, USA, 31 October–2 November 1983, pp.1129–1139.
18. Trinh EH. Compact acoustic levitation device for studies in fluid dynamics and material science in the laboratory and microgravity. *Rev Scient Inst* 1985; 56: 2059–2065.
19. Otsuka T, Higuchi K and Seya K. Ultrasonic levitation by stepped circular vibrating plate. In: *The 10th symposium on ultrasonic electronics*, 1989, p. 170; *Jpn J Appl Phys* 1990; 29: 170–172.
20. Xie WJ and Wei B. Parametric study of single-axis acoustic levitation. *Appl Phys Lett* 2001; 79: 881.
21. Xie WJ, Cao CD, Lu YJ, et al. Acoustic method for levitation of small living animals. *Appl Phys Lett* 2006; 89: 21.
22. Salbu EOJ. Compressible squeeze films and squeeze bearings. *J Basic Eng* 1964; 86: 355–366.
23. Wiesendanger M. *Squeeze film air bearings using piezoelectric bending elements*. PhD Thesis, Ecole Polytechnique Federale de Lausanne, Switzerland, 2001.
24. Michael WA. A gas film lubrication study, Part II: Numerical solution of the Reynolds equation for finite slider bearings. *IBM J* 1959; 3: 256–259.
25. Hamrock BJ. *Fundamentals of fluid film lubrication*. New York: McGraw-Hill Co., 1994.
26. Chu BT and Apfel RE. Response to the comments of Nyborg and Rooney. *Acoust Soc Am* 1984; 75: 1003–1004.
27. Hashimoto Y, Koike Y and Ueha S. Near-field acoustic levitation of planar specimens using flexural vibration. *Acoust Soc Am* 1996; 100: 2057–2061.
28. Nomura H, Kamakura T and Matsuda K. Theoretical and experimental examination of near-field acoustic levitation. *Acoust Soc Am* 2002; 111: 1578–1583.
29. Minikes A, Bucher I and Haber S. Levitation force induced by pressure radiation in gas squeeze films. *Acoust Soc Am* 2004; 116: 217–226.
30. Minikes A and Bucher I. Comparing numerical and analytical solutions for squeeze-film levitation force. *J Fluids Struct* 2006; 22: 713–719.
31. Stolarski TA and Chai W. Inertia effect in squeeze film air contact. *Tribol Int* 2008; 41: 716–723.
32. Woolliscroft CI. *Ultrasonic acoustic levitation*. BEng Report, Brunel University, UK, 2005.
33. Woolliscroft SP. *Investigation into the performance of a self-lifting linear air bearing*. MEng Report, Brunel University, UK, 2005.
34. Taghipourfard M. *Sliding air-contact bearing using acoustic levitation*. BEng Report, Brunel University, UK, 2013.
35. Stolarski TA, Xue Y and Yoshimoto S. Air journal bearing utilizing near field acoustic levitation - Stationary shaft case. *J Eng Tribol* 2011; 225: 120–127.